Acoust. Sci. & Tech. **36**, 2 (2015) ©2015 The Acoustical Society of Japan

PAPER

100-MHz ultrasonic linear array transducers based on polyurea-film

Marie Nakazawa[1,*], Masaya Tabaru[1], Toshiki Takayasu[1], Takahiro Aoyagi[2] and Kentaro Nakamura[1]

[1]*Precision and Intelligence Laboratory, Tokyo Institute of Technology, Nagatsuta-cho 4259, Midori-ku, Yokohama, 226–8503 Japan*
[2]*Graduate School of Decision Science and Technology, Tokyo Institute of Technology, 2–12–1, Ookayama, Meguro-ku, Tokyo, 152–8552 Japan*

(*Received 10 June 2014, Accepted for publication 5 August 2014*)

Abstract: Eight- and 32-element ultrasonic array transducers using polyurea films are fabricated and experimentally tested in this study. Aromatic polyurea thin films, prepared by vapor deposition polymerization, are suitable for use as an ultrasonic transducer. In this paper, we present two types of polyurea array transducer with 20 and 200 μm pitches. The polyurea films were prepared through vapor deposition polymerization, and miniature electrode arrays were fabricated by a lithographic technique. Resonance frequencies of approximately 30, 65, and 100 MHz were observed in the electrical admittance. To examine the performances of the prototype array transducers, a pulse/echo test and phased array experiment were performed. From the experimental results, we found that the polyurea array transducers fabricated by the proposed method correctly operated as expected.

Keywords: Polyurea film, Piezoelectric polymer, High-frequency, Ultrasonic array transducer, Phased array, Lithography

PACS number: 43.35.Ns, 43.38.Ar, 43.38.Fx, 43.38.Hz [doi:10.1250/ast.36.139]

1. INTRODUCTION

High-frequency transducers are required for higher resolution in medical ultrasonic diagnosis [1]. Ultrasound is transmitted and the echo reflected at the boundary of human tissue is received using a single-element or array transducer. High-frequency transducers are also used in photoacoustic imaging to receive photoacoustic signals so that high-resolution images of human tissue can be obtained [2,3]. Several different transducer materials are being investigated for use in high-frequency ultrasound imaging. These include lead zirconate titanate (PZT) [4–8], piezoelectric polymers such as polyvinylidene fluoride (PVDF) [9–11], capacitive micromachined transducers (cMUTs) [12], and zinc oxide (ZnO) [13]. Piezoelectric polymers have drawn considerable attention as materials for advanced transducers [14–17]. Although PVDF [10,11,17] and P(VDF/TrFE) [18,19] have been widely used, there are difficulties in thin-film formation, film thickness control, and shape control for these materials because of the fabrication methods used, which include spin coating and wet processing.

Polyurea (PU) [20], which has very useful characteristics for ultrasonic transducers, has recently been focused on. The preparation method and piezoelectric properties of PU and its applications have been reported [20–29]. The acoustic impedance of PU ($= 3.16 \times 10^6$ N·s·m^{-3}) is close to that of water: therefore, a PU transducer can receive ultrasound with low reflection loss. Since PU are formed by a mask, plural transducers can be produced in one deposition process. The Curie temperature is 200°C, which is the highest value among piezoelectric polymer materials such as PVDF (100°C) or PVD(F-TrFE) (120–180°C) [30]. Thus, by employing a higher frequency with array transducers, higher temporal and spatial resolution can be obtained in imaging applications.

Meanwhile, in general, side lobes are unwanted emissions of ultrasound energy directed away from the main pulse, caused by the radial expansion and contraction of the transducer element. For multielement arrays, side lobe emission occurs in the forward direction along the main beam. By maintaining the individual transducer element pitches at less than half the wavelength, the side lobe emissions are reduced [31]. For example, electric beam focusing can be realized without side lobes at 30 MHz if the array transducer pitch is less than 25 μm.

*e-mail: mtabaru@sonic.pi.titech.ac.jp

We have reported fabrication method of ultrasonic array transducers using PU films [32]. In the report, taking advantage of the features of PU film, prototype 8- and 32-element linear arrays operating at 30, 65, and 100 MHz were fabricated. To produce the array transducers, miniature aluminum electrodes with pitches of 20 and 200 µm were fabricated using a lithographic technique [33]. In this paper, details such as thickness design, fabrication procedure, and evaluation method are reported. In Sect. 2, the fabrication methods of the PU array transducers are described. In Sect. 3.1, to confirm the successful fabrication of the PU array transducers, the admittance characteristics were evaluated. In Sect. 3.2, we verified that the PU array transducer operated correctly by performing a pulse/echo experiment on the 8-element array transducer and a phased array experiment on both types of array transducer.

2. FABRICATION OF ARRAY TRANSDUCERS USING PU FILM

In this section, we describe a fabrication method for high-frequency array transducers using PU film.

2.1. Configuration of Array Transducers

Figure 1(a) shows configuration for the PU array transducers. The array transducers proposed in this paper consist of a top aluminum (Al) electrode, a PU film, bottom Al array electrodes, and a polyimide (PI) substrate. For the fabrication, PU and the top and the bottom Al electrodes were deposited on a PI substrate.

The thicknesses of the Al electrodes and PU film were determined by employing a Mason's equivalent circuit [34]. The thickness of the PU film used in the design is limited, because a PU film tends to crack if its thickness exceeds 6 µm. Therefore, the thickness of the PU film was restricted to less than 6 µm during the deposition process. A combined thickness resonance was used to obtain the fundamental resonance frequency of approximately 30 MHz, because the basic resonance frequency for such a thickness is above 1 GHz. To excite the transducer at a lower frequency and to balance the thick substrate, a thick top electrode of 5 µm Al was applied as a counter mass. Here, we chose Al because the conditions of deposition and etching of Al for our apparatuses had been known for us and we had no experience about other metals.

The designed PU transducer consisted of a top Al electrode (thickness: 5.0 µm), a PU film (thickness: 3.5 µm), a bottom Al electrode (thickness: 0.5 µm), and a PI substrate (thickness: 25 µm). In this configuration, the PU transducer operates with longitudinal vibration between the top surface of the Al electrode and the bottom surface of the Al substrate. According to the result of calculation using Mason's equivalent circuit model, the fundamental, second, and third resonances were appeared at 30, 65, and 101 MHz, respectively. Figure 1(b) shows the calculated amplitudes of the sound pressure and particle velocity inside the designed transducer for use at boundaries between air and air at 30 MHz. The horizontal direction is the vibration direction. The solid and dotted lines indicate the sound pressure and particle velocity, respectively. The PI and the top Al electrode face the air. The figure shows that the pressure and velocity distributions correspond to the half-lambda resonance mode between the top Al electrode and the PI substrate.

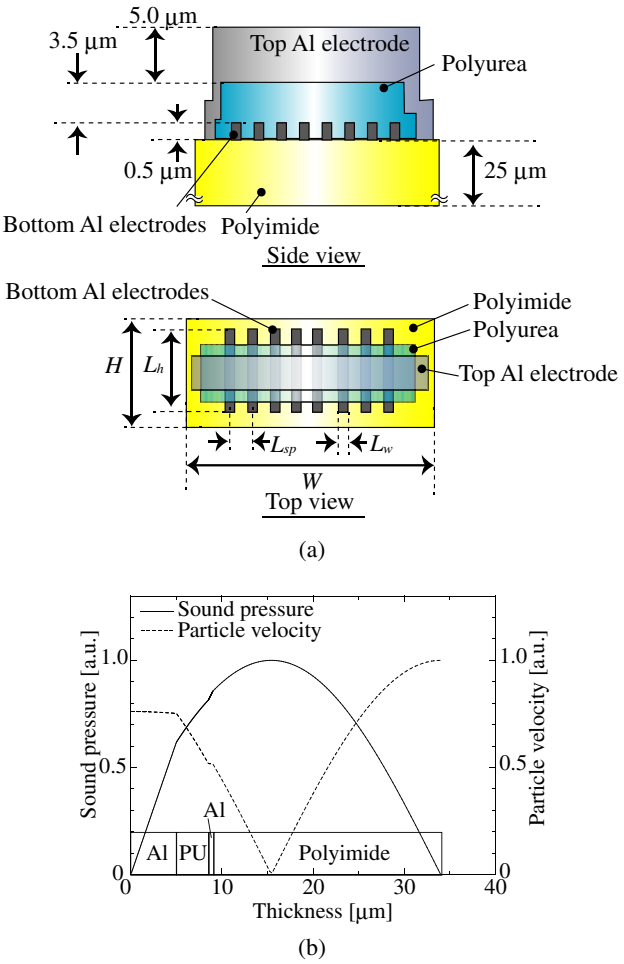

Fig. 1 (a) Configuration of PU array transducer and (b) calculated distributions of sound pressure and particle velocity for PU array transducer at 30 MHz.

For the fabrication of the PU film and the Al electrodes forming the transducer, vacuum deposition equipment was used [24]. A PI substrate was moved between the chambers using belt conveyors to deposit the Al electrodes and the PU film. The PU film and Al electrodes were shaped by masks ($95 \times 115\,mm^2$) located below the substrate. Evaporation rates were monitored using quartz crystal microbalances.

2.2. Mask Pattern of Electrode Arrays

In this work, the bottom electrodes were patterned to form arrays after the deposition process by a lithographic

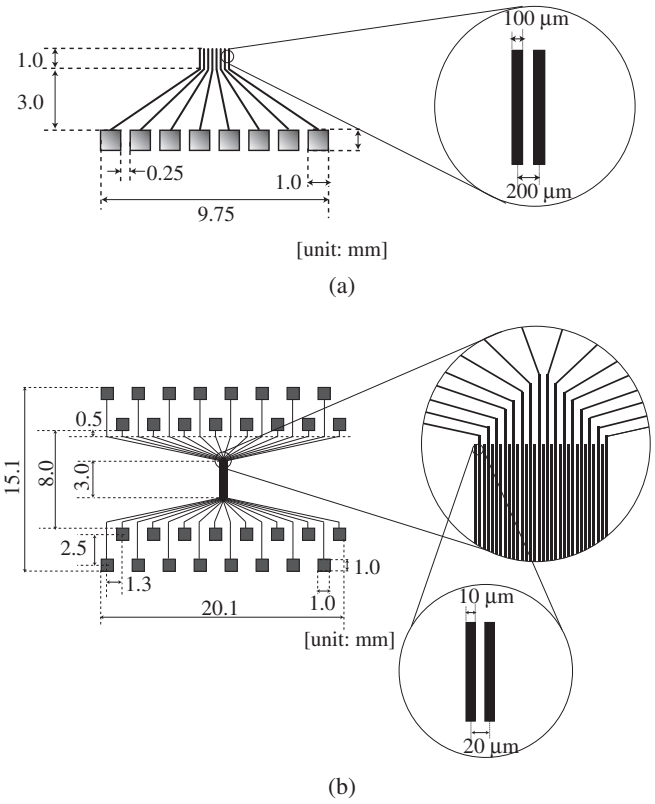

Fig. 2 Mask patterns of the (a) 8- and (b) 32-element electrode arrays with interelement pitches of 200 and 20 µm, respectively.

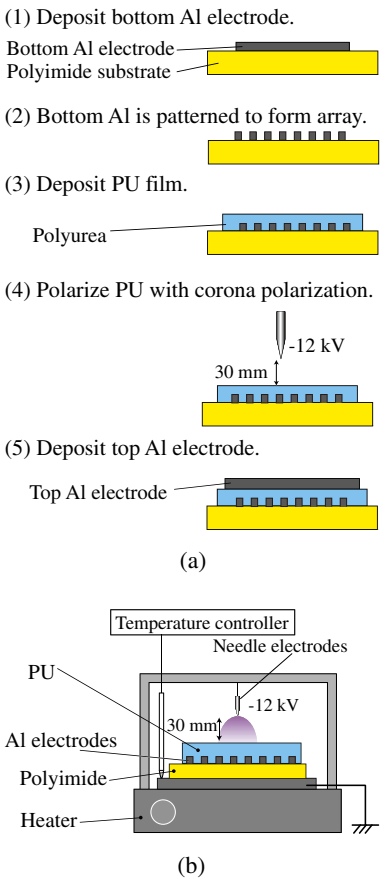

Fig. 3 (a) Fabrication procedure of PU array transducer and (b) setup for corona poling.

technique. As shown in Fig. 2, we fabricated two types of array transducer. The configurations of the electrode arrays for the 8- and 32-element array transducers are shown in Figs. 2(a) and 2(b), respectively. Two types of hard mask were produced for photolithography using an electron beam lithography system (ELIONIX, ELS-6600). Figure 2(a) shows the mask pattern of the 8-element electrode array of 100 µm width L_w and 200 µm pitch L_p, where each element has a height L_h of 1 mm and a thickness of 0.5 µm. Figure 2(b) shows the mask pattern of the 32-element electrode array of 10 µm width L_w and 20 µm pitch L_p, where each element has a height of 3 mm L_h and a thickness of 0.5 µm. Electrode pads of 1 mm^2 are located remotely via leading patterns connected to the effectively vibrating region.

2.3. Fabrication Procedure of PU Array Transducers

Figure 3 shows the proposed fabrication procedure for the PU array transducers.

(1) First, the bottom Al electrodes (thickness, 0.5 µm) were deposited on PI substrates (thickness, 25 µm), with widths W and heights H of 20 mm × 15 mm and 30 mm × 25 mm for the 8- and 32-element array transducers, respectively. Al electrodes were produced using an electron beam gun in the Al deposition chamber.

(2) After the PI films were adhered on other solid substrates using adhesion promoters, liquid adhesion promoters (Tokyo Ohka Kogyo, OAP) and positive photoresists (Tokyo Ohka Kogyo, OFPR-800) were coated (500 rpm for 5 s and 5,000 rpm for 30 s). The photoresist films were then prebaked to remove excess solvents (110°C for 90 s). After prebaking, the photoresists were exposed to ultraviolet (UV) light (30 s) through the electron-beam-patterned hard mask. In this study, the exposure process was performed using a contact-type mask aligner (Karl Suss, MJB3).

The areas of exposed photoresists were removed in a development process (60 s) using developing fluid (Tokyo Ohka Kogyo, NMD-3). The resulting wafers were then postbaked (140°C for 180 s) and the Al electrodes were patterned by wet etching (40°C for 180 s). After gate patternings were performed by etching, the photoresists were removed using acetone. A solution of nitric acid (HNO_3), phosphoric acid (H_3PO_4), and acetic acid (CH_3COOH) (1:16:2) was used for the Al etchant.

(3) Then, PU films of 3.5 µm thickness were deposited on the patterned electrode arrays and the PI substrates using deposition equipment [24]. Polymerization of the PU was carried out through the addition reaction between a

diisocyanate monomer and a diamine monomer. In this study, 4,4′-diphenyl methane diisocyanate (MDI) and 4,4′-diamino diphenyl ether (ODA) were used. To obtain high piezoelectricity, equal quantities of ODA and MDI should be used and the substrate should be kept at 15°C [20,22,35]. In this work, ODA and MDI were evaporated at temperatures of 122 and 62°C, respectively, and the temperature of the substrate was controlled at 15 ± 0.5°C by a Peltier device and a water cooling system.

(4) To polarize the PU films, we applied a corona poling method as shown in Fig. 3(b) [36]. During the corona poling, the PU films were placed 30 mm below a bunch of 15 needles and the PU films were heated at 180°C for 10 min at a voltage of −12 kV. The needles were set above the 8- and 32-element array electrodes. In this setting, the range of polarization is approximately 30–40 mm^2. During the poling process, the Al electrodes tended to exfoliate when the temperature was increased rapidly. This is because of the difference between the thermal expansion coefficients of Al ($= 23 \times 10^{-6}$/K) [37,38] and PU ($= 4$–9×10^{-5}/K) [39]. To suppress the occurrence of exfoliation, the PU films were heated at 180°C for 1 h.

(5) Finally, the top Al electrodes of 5 µm thickness were deposited. This thickness was chosen so that the top electrodes act as a counter mass to acoustically balance the thick substrate. The top electrodes also act as common electrodes for all the bottom electrodes.

2.4. Microscope Images of PU Array Transducers

We fabricated two samples for each type of array transducer. We confirmed the widths of the Al electrode arrays for the fabricated transducers using a digital microscope (KEYENCE, Digital HF Microscope model VH8000C). The microscope images of the 8- and 32-element electrode arrays are shown in Figs. 4(a) and 4(b), respectively. The widths L_w of each element were 100 ± 0.5 µm and 10 ± 0.5 µm for the 8- and 32-element array transducers, respectively. Although disconnected electrodes and electrodes that were a few µm too thin were locally observed for the 32-element array transducer, we confirmed that the array patterns were shaped as designed.

The microscope images of the 8- and 32-element PU array transducers are shown in Figs. 5(a) and 5(b), respectively. The heights of the top electrodes, L_{he}, were 0.9 and 1.0 mm for the 8-element array transducers and 1.5 and 2.5 mm for the 32-element array transducers.

3. EVALUATION OF PU ARRAY TRANSDUCERS

In this section, we report our evaluation of the array transducers formed using PU films.

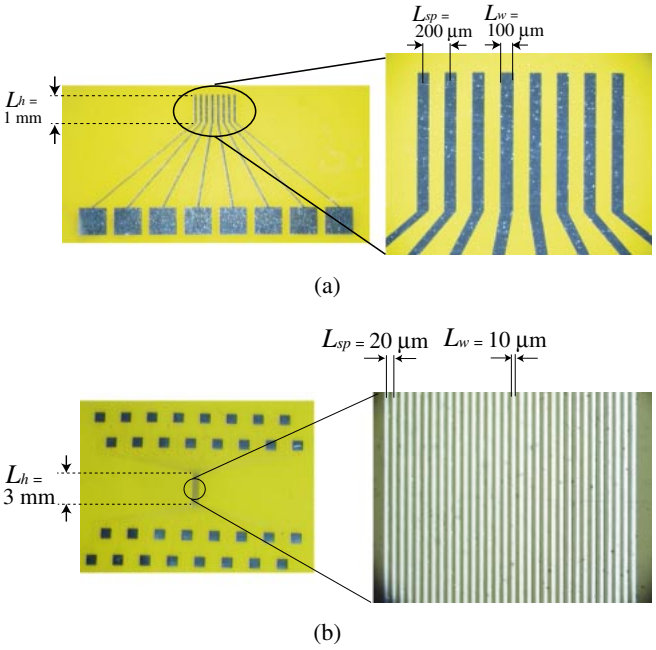

Fig. 4 Microscope images of (a) 8- and (b) 32-element electrode arrays patterned on PI film by wet etching.

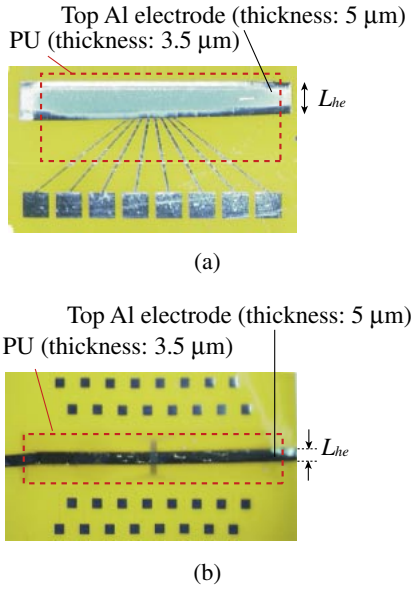

Fig. 5 Microscope images of (a) 8- and (b) 32-element PU array transducer.

3.1. Admittance Characteristics

First, we measured the free admittance characteristics as fundamental characteristics. The free admittances were measured for two samples of each type of array transducer. The admittance characteristics were measured for the 8- and 32-element array transducers using an impedance analyzer (Agilent Technologies, RF Impedance/Material analyzer 4291B). Figure 6 shows the frequency responses of the admittance. We observed longitudinal resonances in the thickness direction at frequencies of 30, 65, and

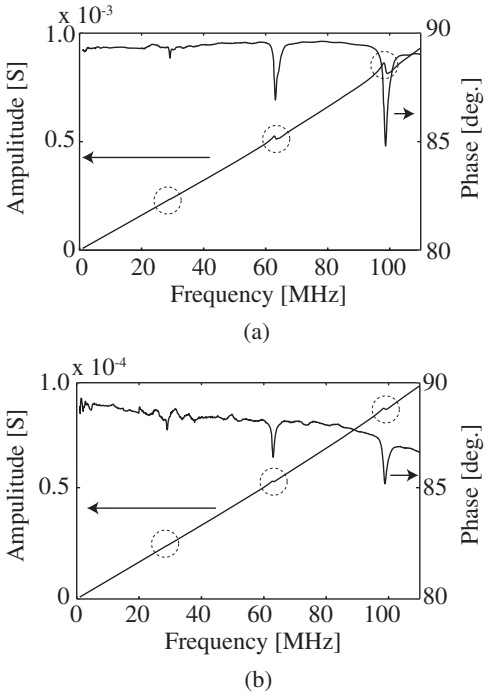

Fig. 6 Admittance characteristics of the (a) 8- and (b) 32-element array transducers.

100 MHz for the array transducers. Table 1 summarizes the frequencies of the maximum conductance f_s and the effective electromechanical coupling coefficient k_{eff} for the fundamental, second, and third resonances. Values of k_{eff} were calculated by

$$k_{eff}^2 = \frac{\pi}{2} \frac{f_s/f_p}{\tan(\pi/2 \cdot f_s/f_p)}, \quad (1)$$

where f_p is the frequency corresponding to the maximum resistance [40]. Frequencies of 30, 65, and 100 MHz were obtained for the fundamental, second, and third resonance frequencies, respectively. As described in Sect. 2.1, the theoretical fundamental, second, and third resonances were found to be at 30, 65, and 101 MHz, respectively, in good agreement with the experimental results. k_{eff} was about 0.10, 0.13, and 0.14 for the fundamental, second, and third resonance frequencies, respectively. The yields were 8/8 and 28/32 for the 8- and 32-element array transducers, respectively.

3.2. Experimental Validation

To experimentally verify the operation of the transducers, we wired the PU array transducers. Figures 7(a) and 7(b) show photographs of the 8- and 32-element array transducers with lead cables (Junkosha, PTFEAWG36 model GT01A040) (7 cables/mm, diameter: 0.15 mm, 1,400 Ω (20°C/km)), respectively. Conductive epoxy (ITW Chemtronics, CW2400) was used to connect the lead cables on the electrode pads. The cables were adhered

Table 1 Admittance characteristics for fundamental, second, and third resonances of the PU array transducers.

Fundamental

Number of elements	sample no.	f_s [MHz]		k_{eff}	
		ave.	std	ave.	std
8	1	30.8	0.060	0.109	0.0144
	2	29.1	0.026	0.107	0.0100
32	1	30.8	0.026	0.096	0.0081
	2	29.0	0.024	0.096	0.0135

Second

Number of elements	sample no.	f_s [MHz]		k_{eff}	
		ave.	std	ave.	std
8	1	65.9	0.098	0.115	0.011
	2	62.8	0.065	0.158	0.009
32	1	66.0	0.047	0.128	0.011
	2	62.8	0.030	0.127	0.009

Third

Number of elements	sample no.	f_s [MHz]		k_{eff}	
		ave.	std	ave.	std
8	1	103.1	0.092	0.126	0.010
	2	98.1	0.130	0.166	0.004
32	1	103.6	0.071	0.148	0.011
	2	98.5	0.075	0.132	0.006

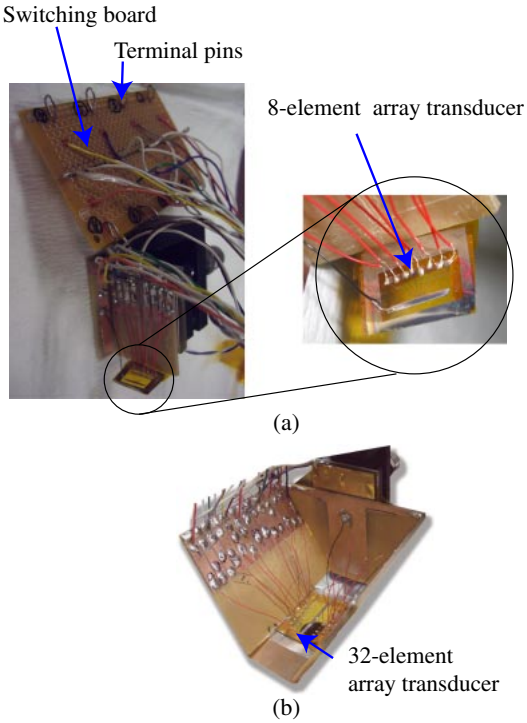

Fig. 7 (a) 8- and (b) 32-element array transducers with lead cables.

at room temperature. The lead cables were soldered on copper-covered bakelite boards. Other cables were soldered on the boards and other bakelite boards for switch-

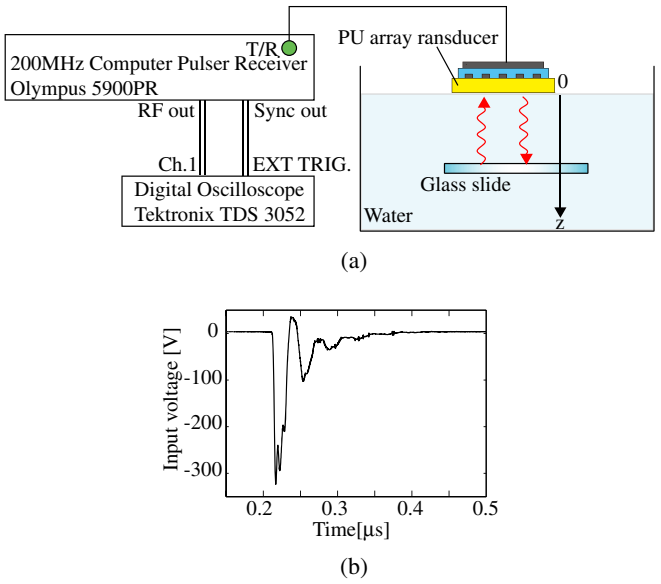

Fig. 8 (a) Experimental setup for pulse/echo experiment with pulsed wave and (b) inputted pulsed waveform.

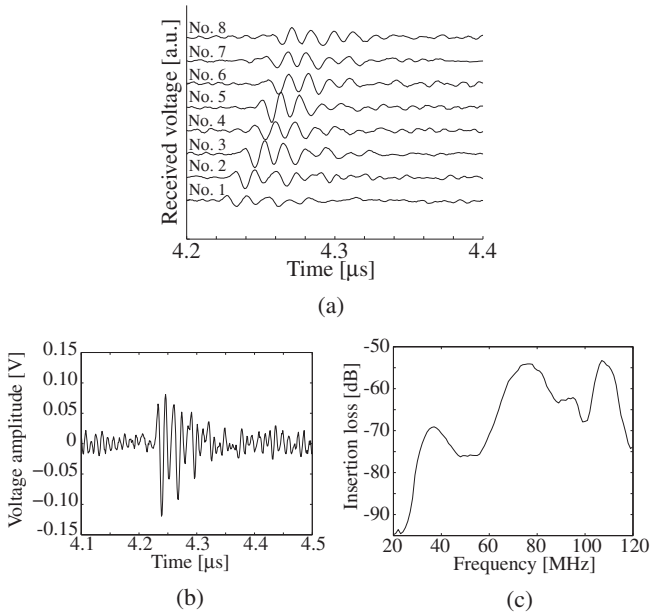

Fig. 9 Results of pulse/echo experiment with the 8-element array transducer: (a) Amplitudes of the reflected waveforms for all the elements. (b) Amplitudes of the reflected waveform and (c) insertion loss for element No. 2.

ing. The input and output signals for each element were controlled by terminal pins on the switching boards.

3.2.1. Pulse/echo test

First, a transmission-reception experiment with a pulsed wave was performed on the 8-element array transducer. The experimental setup is shown in Fig. 8(a). The PU transducer was placed on the surface of degassed water at room temperature, where the back of the PI film was set facing the water. A glass slide of 1 mm thickness was set in the water tank ($100 \times 130 \times 130\,\mathrm{mm}^3$) as a reflector. The position z of the glass slide was controlled by a z-axis stepper motor. The transducer was excited with a pulsed wave of -300 V (Fig. 8(b)) generated by a pulser/receiver (Olympus, Pulser/Receiver model 5900PR, PRF: 200 Hz, damping: 50 Ω, energy: 16 μJ, LPF: 200 MHz, HPF: 10 MHz, gain: 48 dB), where the pulse was transmitted from the bottom of the polyimide substrate. The pulse reflected from the glass slide was received by the same transducer. The resulting pulse was amplified and measured across a 1 MΩ coupling by an oscilloscope (Tektronix, Digital Oscilloscope model TDS 3052). The cable length between the transducer and the pulser/receiver was 1.5 m, and that between the pulser/receiver and the oscilloscope was 1.0 m.

Figure 9(a) shows the received pulse voltages at a distance of $z = 3$ mm. The vertical axis shows the voltage amplitude observed by the oscilloscope and the horizontal axis shows the time after pulse excitation at $t = 0.3$ μs. From Fig. 9(a), we found that each element of the 8-element array transducer could transmit and receive ultrasonic waves. The time delays of 4.2–4.3 μs correspond to the round trips of the ultrasound between the transducer and the object.

Figure 9(b) shows the amplitude of the reflected waveform for element No. 2. The peak-to-peak voltage amplitude was approximately 0.2 V. The pulse length (*PL*), which is defined as the time width at a peak value of -6 dB, was 23.0 ns. The corresponding axial resolution (*AR*) was 17.2 μm. We calculated the insertion loss for the reflected waveforms, which is the transmit/receive voltage from a solid surface relative to the voltage delivered to a 50 Ω resistor in place of the transducer [41–44]. The losses due to attenuation in the water and reflection from the glass slide were subtracted from the measurement. We did not consider losses caused by diffraction. Figure 9(c) shows the calculated insertion loss for element No. 2. The resulting insertion losses (*IL*, -6 dB) for the center frequencies (*CF*) of 37, 76, and 107 MHz were 70, 54, and 53 dB, respectively. The corresponding full widths at half maximum (*FWHM*s, -6 dB) were 18, 17, and 9 MHz, and the relative bandwidths (*RBW*s, -6 dB) were 49, 22, and 8%. The properties of *PW*, *AR*, *CF*, *IL*, *FWHM*, and *RBW* were evaluated for all the elements. The averages and standard deviations of *PW* and *AR* are 33.4 ± 11.5 ns and 25.3 ± 8.6 μs, respectively. The averages and standard deviations of the other properties are shown in Table 2.

The characteristics of the PU array transducer were compared with those of a PVDF array transducer. Carey *et al.* reported average *IL* and *RBW* values of a 20 MHz PVDF array transducer of 59 dB and 113%, respectively

Table 2 Properties of 8-element array transducer.

CF [MHz]		*IL* [dB]		*FWHM* [MHz]		*RBW* [%]	
ave.	std.	ave.	std.	ave.	std.	ave.	std.
36.4	1.1	69.5	1.8	14.4	3.4	39.4	8.4
77.0	2.4	54.0	2.0	25.3	9.6	32.8	12.5
102.6	4.2	58.2	3.5	14.5	6.3	14.3	6.6

[11]. Although *IL* for the PU array transducer was higher than that for the PVDF array transducer at the center frequency of 36 MHz, the *IL*s at the center frequencies of 77 and 103 MHz were lower than that for the PVDF array transducer. All of the *RBW*s of the PU array transducer were less than that of the PVDF array transducer. Since the PU array transducer has a narrow bandwidth, a potential application is the measurement of surface acoustic wave velocity using burst waves of a specific frequency.

3.2.2. Phased array experiment

Next, we performed another experiment to evaluate the reception characteristics of the both types of PU array transducers. As described in Sect. 1, high-frequency transducers are used as sensors. For example, in photoacoustic imaging, the transducers receive photoacoustic signals to obtain high-resolution images of human tissue [2,3].

Figure 10(a) shows the principle of beam steering based on a phased array system [45] with an 8-element array transducer, which was applied in our experiments. Here, we denote the incident angle between the transducer and the wave front of the planar wave as θ. We have the following relationship between θ and the time difference for the τ for the planar wave received at adjacent elements A–H:

$$\theta = \sin^{-1}\left(\frac{c\tau}{L_{\mathrm{sp}}}\right), \tag{2}$$

where c is the sound speed in water (= 1,500 m/s) at room temperature and L_{sp} is the pitch of the array.

The correlation coefficient, $v_{\mathrm{out}}(\tau)$, is expressed as a function of τ:

$$v_{\mathrm{out}}(\tau) = \sum_{n=1}^{m} v_n(t - n\tau). \tag{3}$$

Here, v_n $(n = 1, \cdots, m)$ is the waveform received at element n of the array transducer and m is the total number of elements in the transducer. m is 8 for the case shown in Fig. 10(a). Using Eq. (2), the correlation coefficient is also expressed as a function of θ:

$$v_{\mathrm{out}}(\theta) = \sum_{n=1}^{m} v_n\left(t - \frac{L_{\mathrm{sp}}}{c}\sin\theta \cdot n\right). \tag{4}$$

We can estimate the incident angle by finding θ, which gives the maximum correlation coefficient.

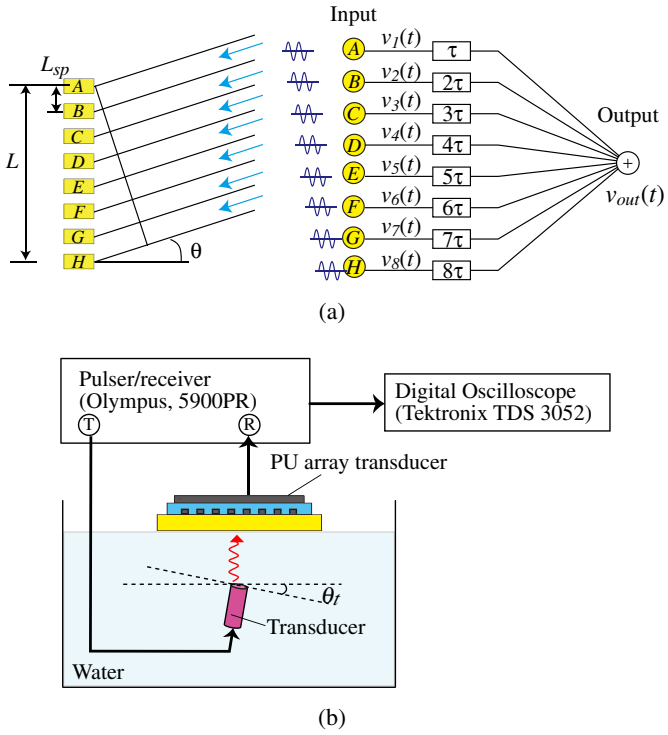

Fig. 10 (a) Principle of phased array system and (b) experimental setup for the phase array experiment.

Figure 10(b) shows the experimental system. We changed the incident angle θ_t, the angle between a single-element transducer and the array transducers. The single-element transducer was rotated using a goniometer. Pulsed ultrasonic waves were radiated by the single-element transducer (flat-type, diameter: 6 mm) with a center frequency of 20 MHz (Olympus, High-Frequency Transducer V354-SU) immersed at the bottom of the water bath. Among the center frequencies of the transducers available in our laboratory, 20 MHz is the closest frequency to the fundamental frequency of the PU array transducer. The array transducers under test were positioned on the water surface, where the back of the PI film was set facing the water. The distance between the two transducers was 2 mm. Their bottom surfaces were illuminated by pulsed waves. The resulting pulse was amplified and measured by the oscilloscope.

The incident angle θ_t was set to 2.0, 3.0, and 4.0° for the 8-element array transducer and 0.6, 2.6, and 3.6° for the 32-element array transducer. We chose adjacent angles so that we could visually distinguish two peaks at different angles using the oscilloscope. The numbers of elements used for the experiments were 8 and 10 for the 8- and 32-element array transducers, respectively. For the 32-element array transducer, 10 elements were alternately chosen.

Figure 11 shows the results. Figures 11(a) and 11(c) show the amplitudes $v_l(t)$ of the received waveforms for various angles for the 8- and 32-element array transducers,

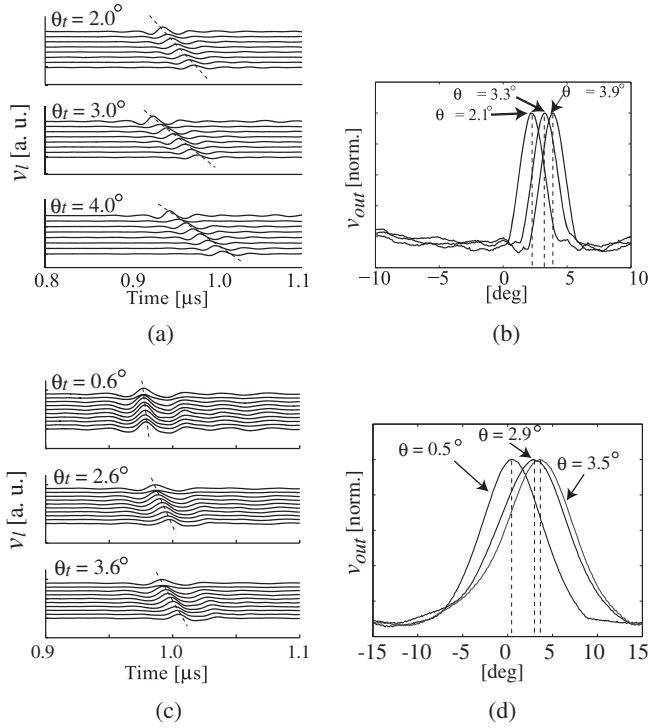

Fig. 11 Results of the phased array experiment. (a) and (c) Amplitudes of the received waveforms for various actual incident angles for the 8- and 32-element array transducers, respectively. (b) and (d) Calculation results for v_{out} for various θ for the (a) 8- and (c) 32-element array transducer, respectively.

respectively. We found that the time difference increased with the actual incident angle. For each received waveform $v_l(t)$, the correlation coefficient $v_{\text{out}}(\theta)$ was calculated as a function of the angle θ using Eq. (4). Figures 11(b) and 11(d) show the calculation results for $v_{\text{out}}(\theta)$ for the 8- and 32-element array transducers, respectively. The incident angles were then estimated by finding the maximums values of v_{out} in Figs. 11(b) and 11(d) for the actual incident angles. The incident angles estimated from the phased array experiment were 2.1, 3.3, and 3.9° for the 8-element array transducer and 0.5, 2.9, and 3.5° for the 32-element array transducer. The estimated angles were in good agreement with the actual angles. The estimation errors were less than 10% for the 8-element array transducer and less than 11% for the 32-element array transducer.

The values of v_{out} shown in Figs. 11(b) and 11(d) indicate the beam width of the array transducers. To verify the beam width, we compared the beam width at half maximum BW in Figs. 11(b) and 11(d) with the theoretical width (−6 dB) at normal incidence calculated from the beam pattern of an array transducer [31]. The theoretical beam pattern $p(\theta)$ was given by

$$p(\theta) = \frac{\sin^2(kL\sin\theta/2)}{(kL\sin\theta/2)^2}. \quad (5)$$

Here, k is the wave number and L is the total width of the array aperture illustrated in Fig. 10(a). The theoretical beam width was 2.5° for the 8-element array transducer. The estimated BWs were 2.4, 2.4, and 2.3° for incident angles of 2.0, 3.0, and 4.0°, respectively. The experimental results were good agreement with the theoretical value for the 8-element array. For the 32-element array transducer, the theoretical value was 8.2°, and the estimated BWs were 8.4, 9.6, and 9.2° for incident angles of 0.6, 2.6, and 3.6°, respectively. The estimation errors were less than 8% for the 8-element array transducer and less than 17% for the 32-element array transducer. From the experimental results, we found that the PU array transducers fabricated by the proposed method correctly operated as expected.

4. CONCLUSION

In this study we studied PU-film ultrasonic array transducers. We proposed a fabrication method for high-frequency array transducers using PU film. Eight-element bottom electrode arrays with 200 μm pitch and 32-element bottom electrode arrays with 20 μm pitch were patterned on polyimide substrates by a photolithographic technique. The array transducers were fabricated by depositing PU films and top electrodes using deposition equipment, which was followed by corona poling.

The yields of the 8- and 32-element array transducers were 100 and 88%, respectively. The array transducers showed resonances at approximately 30, 65, and 100 MHz and effective electromechanical coupling coefficients of 0.10–0.17. We successfully estimated the incident angles in a phased array experiment. In addition, we observed reflected pulse signals in a pulse/echo experiment using the 8-element array transducer. From these validation experiments, we found that the fabricated PU array transducers correctly operated as expected. In future works, we will consider how to improve the effective electromechanical coupling coefficient and the sensitivity of the PU array transducer as well as the fabrication process. We used Al as electrodes in this study, however, other materials might be preferable. Optimum materials will be also investigated.

ACKNOWLEDGEMENTS

The authors would like to thank Yoshiyuki Oono, Akihiro Matsutani, and Siro Hino for their assistance with the lithography. Authors are indebted to insightful suggestions and continuous encouragement by Professor Sadayuki Ueha for conducting this work. This work was partly supported by Japan Society for the Promotion of Science (17-8595).

REFERENCES

[1] G. R. Lockwood, D. H. Turnbull, D. A. Christopher and F. S. Foster, "Beyond 30 MHz: Applications of high frequency

ultrasonic imaging," *IEEE Eng. Med. Biol.*, **15**(6), pp. 60–71 (1996).

[2] K. Maslov, G. Stoica and L. V. Wang, "*In vivo* dark-field reflection-mode photoacoustic microscopy," *Opt. Lett.*, **30**, 625–627 (2005).

[3] C. Zhang, K. Maslov and L. V. Wang, "Subwavelength-resolution label-free photoacoustic microscopy of optical absorption *in vivo*," *Opt. Lett.*, **35**, 3195–3197 (2010).

[4] J. M. Cannata, T. A. Ritter and K. K. Shung, "A 35 MHz linear array for medical imaging," *Proc. IEEE Ultrason. Symp.*, pp. 1157–1160 (2001).

[5] T. A. Ritter, T. R. Shrout and K. K. Shung, "Development of high frequency medical ultrasound arrays," *Proc. IEEE Ultrason. Symp.*, pp. 1127–1133 (2001).

[6] F. Akasheh, T. Myers, J. D. Fraser, S. Bose and A. Bandyopadhyay, "Development of piezoelectric micromachined ultrasonic transducers," *Sens. Actuators*, **111**, 275–287 (2004).

[7] D. E. Dausch, J. B. Castellucci, D. R. Chou and O. T. von Ramm, "Piezoelectric micromachined ultrasound transducer (pMUT) arrays for 3D imaging probes," *Proc. IEEE Ultrason. Symp.*, pp. 930–933 (2006).

[8] K. Otsu, S. Yoshizawa and S. Umemura, "Therapeutic array transducer element using coresonance between hemispherical piezoceramic shell and water sphere: Effect of load masses of support and electric contact," *Jpn. J. Appl. Phys.*, **51**, 07GF24 (2012).

[9] K. Kimura, N. Hashimoto and H. Ohigashi, "Performance of a linear array transducer of vinylidene fluoride trifluoroethylene copolymer," *IEEE Trans. Sonics Ultrason.*, **32**, 566–573 (1985).

[10] S. J. Carey, C. M. Gregory, M. P. Brewin, M. J. Birch, S. Ng and J. V. Hatfield, "PVdF array characterisation for high frequency ultrasonic imaging," *Proc. IEEE Ultrason. Symp.*, pp. 1930–1933 (2004).

[11] S. J. Carey, C. Brox-Nilsen, H. M. Lewis, C. M. Gregory and J. V. Hatfield, "Scanning head with 128-element 20-MHz PVDF linear array transducer," *IEEE Trans. Ultrason. Ferroelectr. Freq. Control*, **56**, 1769–1777 (2009).

[12] X. Jin, Ö. Oralkan, F. L. Degertekin and B. T. Khuri-Yakub, "Characterization of one-dimensional capacitive micromachined ultrasonic immersion transducer arrays," *IEEE Trans. Ultrason. Ferroelectr. Freq. Control*, **48**, 750–760 (2001).

[13] S. Takayanagi, T. Yanagitani and M. Matsukawa, "Wideband multimode transducer consisting of *c*-axis tilted ZnO/*c*-axis normal ZnO multilayer," *Jpn. J. Appl. Phys.*, **51**(7S), 07GC08 (2012).

[14] T. T. Wang, J. M. Herbert and A. M. Glass, Eds., *The Application of Ferroelectric Polymers*, (Chapman and Hall, New York, 1988).

[15] I. Seo, "Piezoelectricity of vinylidene cyanide copolymers and their applications," *Ferroelectrics*, **171**, 45–55 (1995).

[16] K. K. Shung and M. Zippuro, "Ultrasonic transducers and arrays," *IEEE Eng. Med. Biol. Mag.*, **15**(6), pp. 20–30 (1996).

[17] F. S. Foster, K. A. Harasiewicz and M. D. Sherar, "A history of medical and biological imaging with polyvinylidene fluoride (PVDF) transducers," *IEEE Trans. Ultrason. Ferroelectr. Freq. Control*, **47**, 1363–1371 (2000).

[18] K. Snook, S. Rhee, M. Robert, E. Gottlieb and K. K. Shung, "Development of P(VDF-TrFE) ultrasonic transducers operating at 50–120 MHz," *Proc. IEEE Ultrason. Symp.*, pp. 1249–1252 (2002).

[19] M. Robert, G. Molingou, K. Snook, J. Cannata and K. K. Shung, "Fabrication of focused poly(vinylidene fluoridetrifluoroethylene) P(VDF-TrFE) copolymer 40–50 MHz ultrasonic transducers on curved surfaces," *J. Appl. Phys.*, **96**, 252–256 (2004).

[20] Y. Takahashi, S. Ukishima, M. Iijima and E. Fukada, "Piezoelectric properties of thin films of aromatic polyurea prepared by vapor deposition polymerization," *J. Appl. Phys.*, **70**, 6983–6987 (1991).

[21] Y. Takahashi, M. Iijima and E. Fukada, "Pyroelectricity in poled thin films of aromatic polyurea prepared by vapor deposition polymerization," *Jpn. J. Appl. Phys.*, **28**, 2245–2247 (1989).

[22] X. Wang, Y. Takahashi, M. Iijima and E. Fukada, "Dependence of piezoelectric and pyroelectric activities of aromatic polyurea thin films on monomer composition ratio," *Jpn. J. Appl. Phys.*, **32**, 2768–2773 (1993).

[23] X. Wang, Y. Takahashi, M. Iijima and E. Fukada, "Piezoelectric and dielectric properties of aromatic polyurea synthesized by vapor deposition polymerization," *Jpn. J. Appl. Phys.*, **34**, 1585–1590 (1995).

[24] M. Nakazawa, T. Kosugi, H. Nagatsuka, A. Maezawa, K. Nakamura and S. Ueha, "Polyurea thin film ultrasonic transducers for nondestructive testing and medical imaging," *IEEE Trans. Ultrason. Ferroelectr. Freq. Control*, **54**, 2165–2174 (2007).

[25] M. Nakazawa, M. Tabaru, K. Nakamura, S. Ueha and A. Maezawa, "Multilayered transducers using polyurea film," *Jpn. J. Appl. Phys.*, **46**, 4466–4473 (2007).

[26] T. Aoyagi, M. Nakazawa, K. Nakamura and S. Ueha, "Numerical analysis of ultrasonic beam of variable-line-focus-beam film transducer," *Jpn. J. Appl. Phys.*, **46**, 4486–4489 (2007).

[27] T. Aoyagi, M. Nakazawa, M. Tabaru, K. Nakamura and S. Ueha, "Measurement of surface acoustic wave velocity using a variable-line-focus polyurea thin-film ultrasonic transducer," *IEEE Trans. Ultrason. Ferroelectr. Freq. Control*, **56**, 1761–1768 (2009).

[28] M. Nakazawa, M. Tabaru, T. Aoyagi, K. Nakamura and S. Ueha, "Thickness design, fabrication, and evaluation of 100-MHz polyurea ultrasonic transducer," *IEEE Trans. Ultrason. Ferroelectr. Freq. Control*, **60**, 2175–2188 (2013).

[29] M. Tabaru, M. Nakazawa, K. Nakamura and S. Ueha, "Three-axis acceleration sensor using polyurea films," *Jpn. J. Appl. Phys.*, **47**, 4044–4047 (2008).

[30] H. Ohigashi, *Cho-onpa Binran* (*Handbook of Ultrasonic Wave*), K. Nakamura, Ed. (Maruzen, Tokyo, 1999), (in Japanese).

[31] D. A. Christensen, *Ultrasonic Bioinstrumentation* (Wiley, New York, 1988).

[32] T. Takayasu, M. Nakazawa, K. Nakamura and S. Ueha, "A 100-MHz 32-array transducer using lithographically-made electrodes and vapor-deposited polyurea filmz," *Proc. IEEE Ultrason. Symp.*, pp. 1773–1776 (2008).

[33] C. Mack, *Fundamental Principles of Optical Lithography: The Science of Microfabrication* (Wiley, New York, 2007).

[34] T. Aoyagi, D. Koyama, K. Nakamura and M. Nakazawa, "Equivalent circuit analysis and design of multilayered polyurea ultrasonic transducers," *Jpn. J. Appl. Phys.*, **49**(7S), 07HD05 (2010).

[35] S. Ukishima, T. Takao, M. Iijima, Y. Takahashi, S. Tsukahara and E. Fukada, "Piezoelectric and pyroelectric properties of poled thin films of aromatic polyurea prepared by vapor deposition polymerization," *Proc. 31st Annu. Symp. Vacuum Society of Japan*, pp. 358–360 (1991).

[36] M. Iijima, S. Ukishima, K. Iida, Y. Takahashi and E. Fukada, "Fourier transform infra red observation of the orientation of dipolar urea bonds in polyurea during corona poling," *Jpn. J.*

Appl. Phys., **34**, 65–68 (1995).
[37] E. R. Cohen, D. R. Lide and G. L. Trigg, Eds., *AlP Physics Desk Reference*, 3rd ed. (Springer, New York, 2003).
[38] D. R. Lide, Ed., *CRC Handbook of Chemistry and Physics*, 88th ed. (Taylor & Francis Group, Florida, 2008).
[39] M. Biron, *Thermosets and Composites: Technical Information for Plastics Users* (Elsevier, Oxford, 2004).
[40] *IEEE standard on piezoelectricity*, ANSI/IEEE Standard 176 (1987).
[41] M. D. Sherar and F. S. Foster, "The design and fabrication of high frequency poly(vinylidene fluoride) transducers," *Ultrason. Imag.*, **11**, 75–94 (1989).
[42] G. R. Lockwood and F. S. Foster, "Modeling and optimization of high-frequency ultrasound transducers," *IEEE Trans. Ultrason. Ferroelectr. Freq. Control*, **41**, 225–230 (1994).
[43] K. A. Snook, J. Zhao, C. H. F. Alves, J. M. Cannata, W. Chen, R. J. Meyer, Jr., T. A. Ritter and K. K. Shung, "Design, fabrication, and evaluation of high frequency, single-element transducers incorporating different materials," *IEEE Trans. Ultrason. Ferroelectr. Freq. Control*, **49**, 169–176 (2002).
[44] J. M. Cannata, T. A. Ritter, W. Chen, R. H. Silverman and K. K. Shung, "Design of efficient, broadband single-element (20–80 MHz) ultrasonic transducers for medical imaging applications," *IEEE Trans. Ultrason. Ferroelectr. Freq. Control*, **50**, 1548–1557 (2003).
[45] K. Nakamura and K. Fukaya, "Optical fiber coupler array for multi-point sound field measurement," *Opt. Rev.*, **4**, 65–68 (1997).